OPERA

OPERA Algorithm Theoretical Basis Document for Radiometric Terrain-Corrected SAR Backscatter from Sentinel-1 Product

Version 1.0

JPL D-107393, Initial

June 25, 2024

URS CL#25-1683

Paper copies of this document may not be current and should not be relied on for official purposes.

Authors: Gustavo H. X. Shiroma and Heresh Fattahi

Jet Propulsion Laboratory
California Institute of Technology

SIGNATURE PAGE

Prepared by:

Electronic Signatures in EPDM

Gustavo H. X. Shiroma
OPERA RTC-S1 Product Lead

Date

Electronic Signatures in EPDM

Heresh Fattahi
Project Sub-Element Manager for OPERA Algorithms

Date

Approved by:

Electronic Signatures in EPDM

Luca Cinquini
OPERA Project Manager

Date

Electronic Signatures in EPDM

Steven Lewis
OPERA Project System Engineer

Date

Electronic Signatures in EPDM

Steven Chan
OPERA Project Scientist

Date

ELECTRONIC SIGNATURES IN EPDM

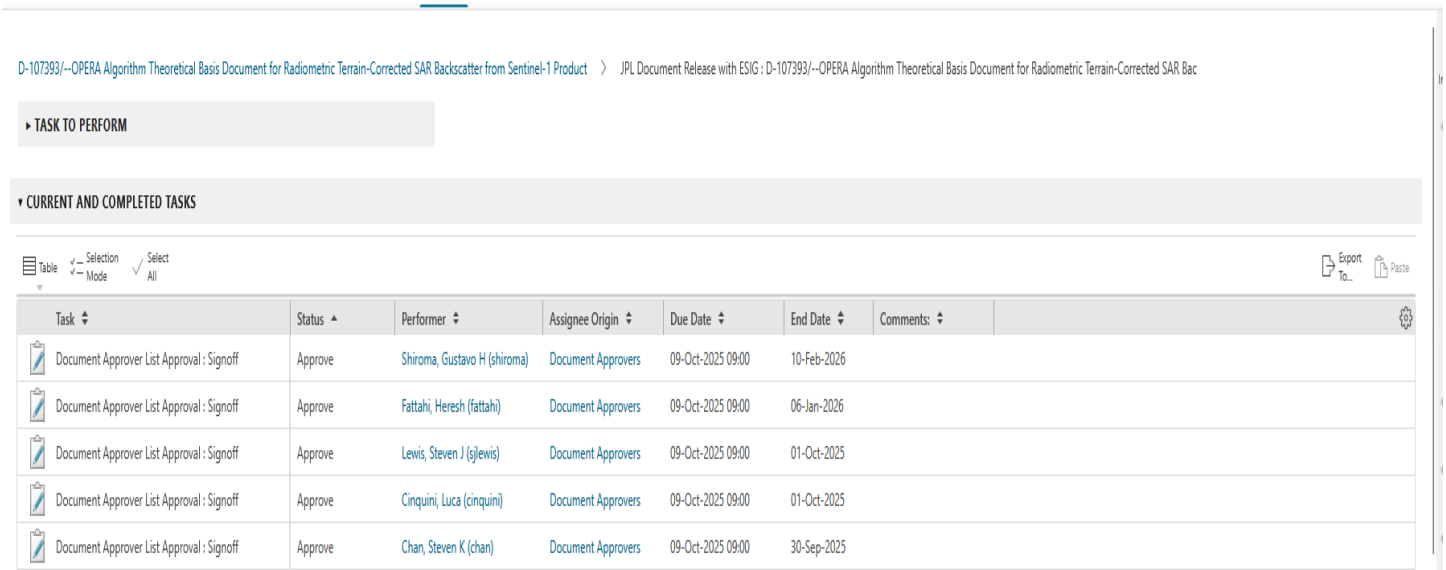

D-107393/--OPERA Algorithm Theoretical Basis Document for Radiometric Terrain-Corrected SAR Backscatter from Sentinel-1 Product 〉 JPL Document Release with ESIG : D-107393/--OPERA Algorithm Theoretical Basis Document for Radiometric Terrain-Corrected SAR Bac

▸ TASK TO PERFORM

▾ CURRENT AND COMPLETED TASKS

Table | Selection Mode | Select All | Export To... | Paste

Task	Status	Performer	Assignee Origin	Due Date	End Date	Comments:
Document Approver List Approval : Signoff	Approve	Shiroma, Gustavo H (shiroma)	Document Approvers	09-Oct-2025 09:00	10-Feb-2026	
Document Approver List Approval : Signoff	Approve	Fattahi, Heresh (fattahi)	Document Approvers	09-Oct-2025 09:00	06-Jan-2026	
Document Approver List Approval : Signoff	Approve	Lewis, Steven J (sjlewis)	Document Approvers	09-Oct-2025 09:00	01-Oct-2025	
Document Approver List Approval : Signoff	Approve	Cinquini, Luca (cinquini)	Document Approvers	09-Oct-2025 09:00	01-Oct-2025	
Document Approver List Approval : Signoff	Approve	Chan, Steven K (chan)	Document Approvers	09-Oct-2025 09:00	30-Sep-2025	

DOCUMENT CHANGE LOG

Revision	Cover Date	Sections Changed	ECR #	Reason, ECR Title, LRS #*
Preliminary	September 12, 2022	All	N/A	New document, LRS# LRR067540
v1.0	June 25, 2024	All	N/A	Update for v1.0. URS CL#25-1683

* *Include the JPL Limited Release System (LRS) clearance number for each revision to be shared with foreign partners.*

TABLE OF CONTENTS

1 INTRODUCTION AND BACKGROUND

1.1 Purpose of Document

This Algorithm Theoretical Basis Document (ATBD) provides the theoretical basis for the algorithms used to create the Observational Products for End-Users from Remote Sensing Analysis (OPERA) Radiometric Terrain-Corrected Synthetic Aperture Radar (SAR) Backscatter from Sentinel-1 (RTC-S1) product. The OPERA RTC-S1 product is derived from Copernicus Sentinel-1 (S1) SAR data, provided by the European Space Agency (ESA). The OPERA Algorithm Development Team (ADT) implements these algorithms in the Science Algorithm Software (SAS) and provides the SAS to the OPERA Science Data System (SDS) for generation of OPERA RTC-S1 products.

1.2 Product Overview

The OPERA RTC-S1 product provides map-projected burst-based radar images derived from the Copernicus Sentinel-1 single-look complex (SLC) data and normalized to gamma-naught γ^0. A visual representation of the OPERA RTC-S1 product is shown in Fig. 1-1.

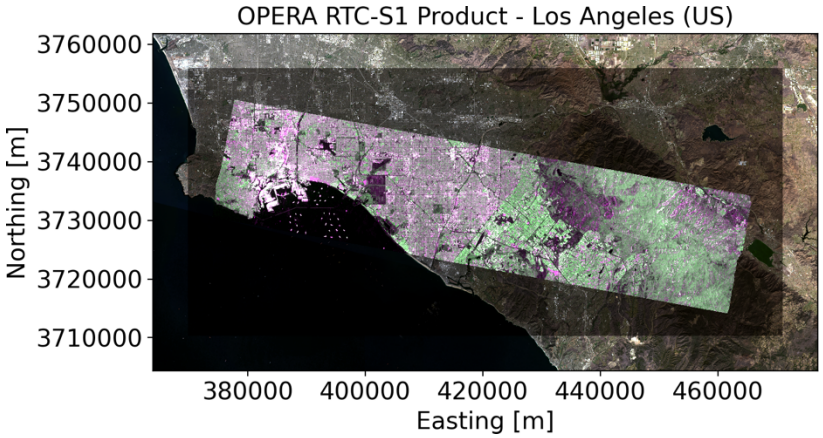

Figure 1-1-1 OPERA RTC-S1 product from Sentinel-1B acquired over Los Angeles (US) on Nov. 20, 2021. The radar backscatter is represented by a red, green, and blue (RGB) composition of VV (red), VH (green), VV (blue), ranging from 0 to 0.44 (VV) and 0.08 (VH).

The spatial coverage of the standard OPERA RTC-S1 product is near-global with a geographic scope that includes all land masses excluding Antarctica, and with temporal sampling coincident with the availability of Sentinel-1 interferometric wide (IW) single-look complex (SLC) data. The RTC-S1 product is projected over Universal Transverse Mercator (UTM) or National Snow and Ice Data Center (NSIDC) Sea Ice Polar Stereographic North coordinates systems. The map grid for each RTC-S1 product is pre-defined based on the S1 burst identification (burst ID). All RTC-S1 products sharing the same burst ID have exact same geographic grid, facilitating data

access and handling from end users. The reference digital elevation model (DEM) utilized in the processing of the RTC-S1 product is based on the Copernicus DEM 30-m (GLO-30) and 90-m (GLO-90), provided by the European Space Agency (ESA).

The RTC-S1 imagery are distributed as single-band cloud-optimized GeoTIFFs (COGs). These files are populated with relevant metadata following GeoTIFF specifications. A separate file containing more complete metadata is provided in the Hierarchical Data Format 5 (HDF5) format following Climate and Forecast (CF) Conventions 1.8.

Radar-geometry layers such as incidence angle, local incidence angle, layover/shadow mask, and radiometric terrain correction (RTC) gamma-to-beta and gamma-to-sigma factors vary slightly over time for each position on the ground [Agram et all, 2023], and therefore are considered static for the project. These static layers are provided separately from the RTC-S1 product as the OPERA RTC-S1 static layers (RTC-S1-STATIC) product. RTC-S1-STATIC products are produced only once or a limited number of times, to account for changes in the S1 orbit, in the DEM, or in the static-layers generation algorithm. RTC-S1-STATIC products are provided with map grid matching RTC-S1 products with the same burst ID.

A global mosaic of RTC-S1 products resulting from a single Sentinel-1A orbit cycle is shown in Figure 1-2. The mosaic is over RTC-S1 products produced by a global end-to-end run test performed by the OPERA SDS with Sentinel-1A data acquired between April 11, 2021 and to April 22, 2021 (12 days). The mosaic was generated from merging a global mosaic of VV+VH and VV-only acquisitions with missing values covered with a polar mosaic of HH+HV and HH-only observations.

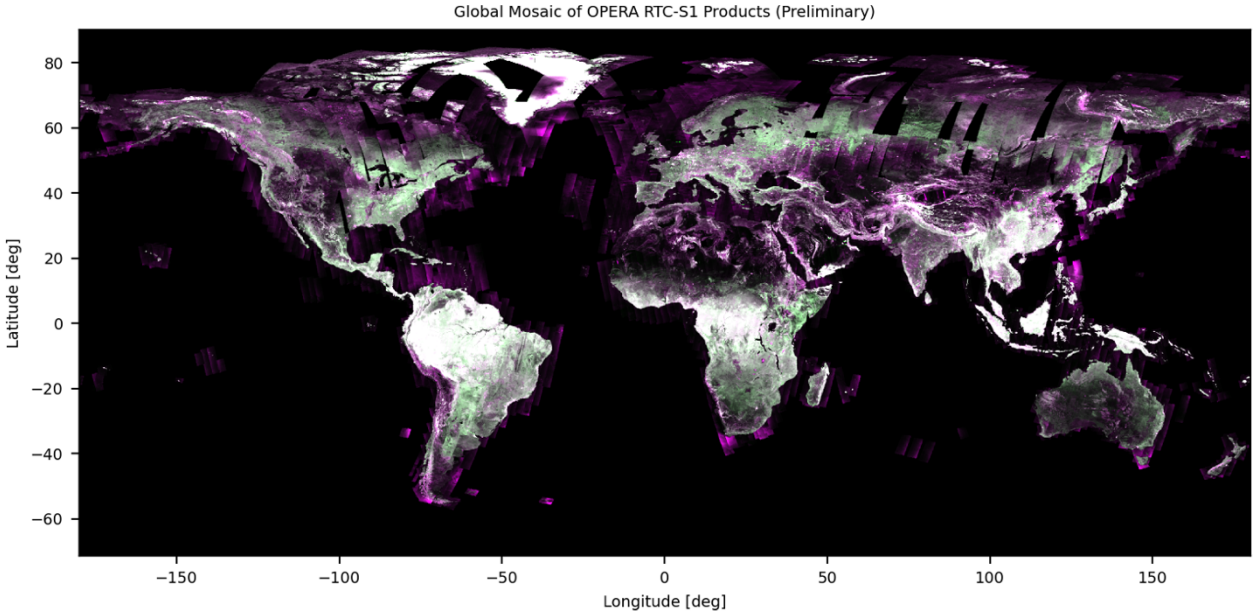

Figure 1-2. Global mosaic of preliminary RTC-S1 products represented by an RGB-color composition of co-polarimetric channels in red and blue colors, and cross-polarimetric channels in green color. The mosaic was generated from merging a global mosaic of VV+VH and VV-only acquisitions with missing values covered with a polar mosaic of HH+HV and HH-only observations. Co- and cross polarimetric backscatter values range from 0 to 0.17 and from 0 to 0.035, respectively.

2 ALGORITHM DESCRIPTION

2.1 Overview of the RTC-S1 Algorithm

The workflow for RTC from Sentinel-1 SLC products, hereafter referred to as OPERA RTC workflow, relies on an area-based projection (AP) algorithm developed for the NASA-ISRO Synthetic Aperture Radar (NISAR) mission, and implemented within the open-source InSAR Scientific Computing Environment Enhanced Edition (ISCE3) framework [Shiroma et al., 2022].

The OPERA RTC workflow consists of two main steps:

1. Area-based radiometric terrain correction (RTC-AP);
2. Geocoding with adaptive multilooking (GEO-AP).

The improved geocoding replaces the traditional workflow with constant-window multilooking followed by geocoding with interpolation into a single geocoding step, performed after the radiometric terrain correction (Fig. 2-1).

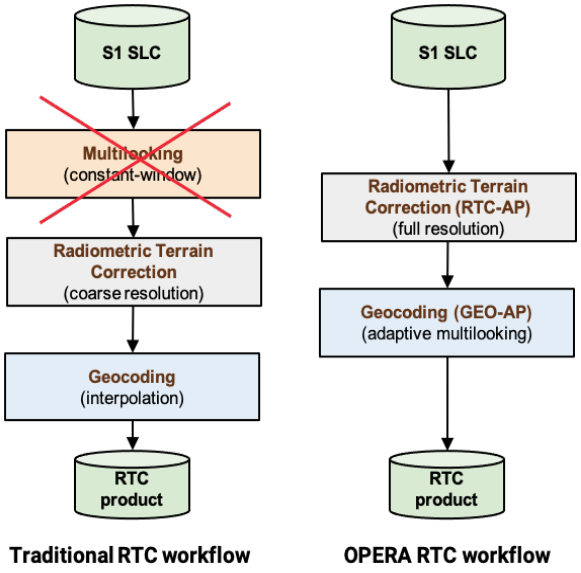

Figure 2-1.(Left) Traditional workflow for generating RTC images and (Right) new OPERA RTC workflow.

2.2 The OPERA RTC-S1 Algorithm

2.2.1 Pre-Processing

Sentinel-1 SLCs are represented as complex *Digital Numbers* (DNs). The first step of the RTC-S1 workflow consists of converting DNs into radar brightness β^0 through an *absolute radiometric correction* [Miranda and Meadows, 2015], and subsequently, the β^0 backscatter coefficient is corrected for *thermal noise* [Piantanida et al., 2017]. The azimuth and range shifts due to bistatic [Gisinger et al., 2021] and static-tropospheric delays [Breit et al., 2010] are computed as look-up tables (LUTs). The resulting thermal-noise corrected β^0 backscatter and azimuth and range delay LUTs are then passed to ISCE3 for radiometric terrain correction and geocoding.

2.2.2 Radiometric Terrain Correction

The radiometric terrain correction normalizes β^0backscatter coefficient at full SLC-resolution into γ^0 (Figure 2-2). The coefficient γ^0 is chosen to minimize the variation of the backscatter coefficient with terrain slope [Ulaby et al., 1986], as shown in Figure 2-2.

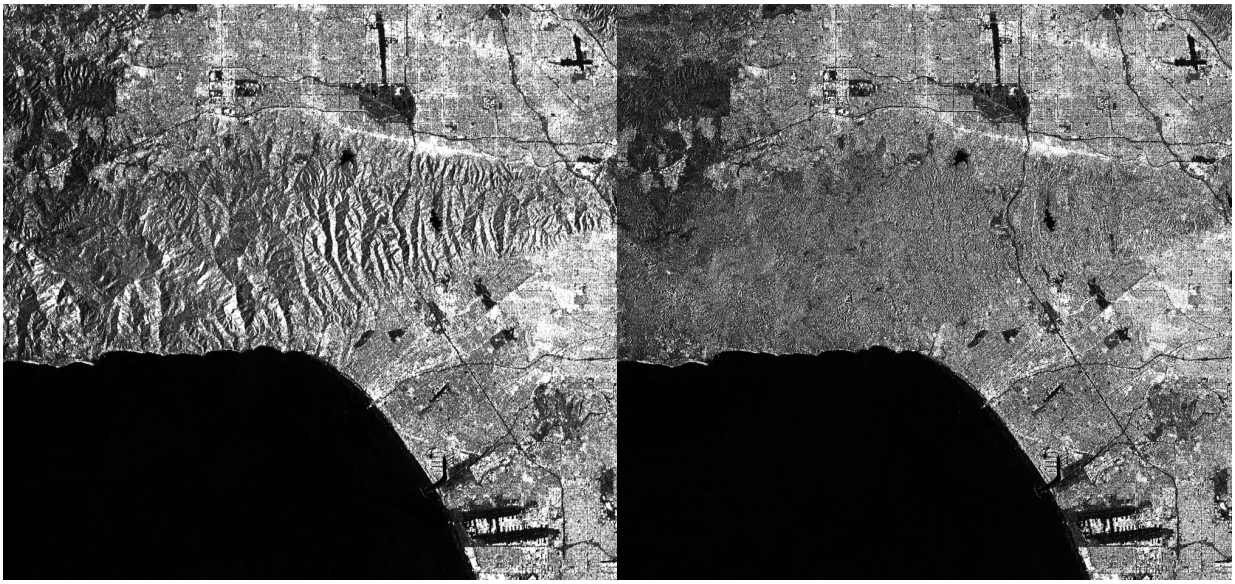

Figure 2-2. Geocoded (Left) beta-naught and (Right) gamma-naught backscatter (VV) from the Sentinel-1B Southern California dataset generated with the suggested workflow with area projection algorithm (ISCE3-AP). The area covers the Santa Monica Mountains in Greater Los Angeles. The radiometric terrain correction with the area projection algorithm (RTC-AP) corrects the radar backscatter for the effects of the terrain. The workflow also employs the area projection algorithm for geocoding (GEO-AP) providing an improved map projection with an adaptive multilooking. The color scale varies from 0 (black) to 0.35 (white).

2.2.3 Theoretical Background

SAR radiometric correction is the process of retrieving the radar cross section (RCS) of a point target or a backscatter coefficient of a distributed target normalized to a reference area [Ulander, 1996, D. Small, 2011]. The backscatter coefficients radar brightness β^0, sigma-naught σ^0, and gamma-naught γ^0 represent the radar cross-section normalized to three reference surfaces: image reference surface A_β, ground surface A_σ, and cross-section reference surface A_γ [Ulander, 1996; Small, 2001, Shiroma et al., 2022], according to the acquisition geometry and the local topography, as shown in Fig. 2-3 [Shiroma et al., 2022]. All three backscatter coefficients are unitless.

SAR SLC images are typically distributed as either beta-naught, β^0, or sigma-naught σ_e^0, also known as the sigma-naught-ellipsoid or ellipsoidal sigma-naught, calculated using the incidence angle θ, which is the angle between the look vector and the geodetic vertical normal to the ellipsoid, according to

$$\sigma_e^0 = \beta^0 \, sin\, \theta \; = \beta^0 \frac{A_\beta}{A_{\sigma_e}} \tag{1}$$

Sentinel-1 SLCs are distributed as beta-naught β^0. The backscatter coefficients σ^0 and γ^0 are obtained for each image sample following the equations:

$$\sigma^0 = \beta^0 \, cos\, \psi \; = \beta^0 \frac{A_\beta}{A_\sigma} \tag{2}$$

$$\gamma^0 = \beta^0 \frac{cos\;\psi}{cos\;\theta_i} = \beta^0 \frac{A_\beta}{A_\gamma} \tag{3}$$

where θ_i is the local incidence angle defined as the angle between the unit vector normal to the local terrain slope $\hat{n}$ and the unit vector pointing from the target to the radar platform $\hat{r}$:

$$\theta_i = \text{acos}(\hat{n} \cdot \hat{r}) \tag{4}$$

The projection angle ψ is the angle between the normal to the image plane $\hat{g}$ (obtained as outer product between $\hat{r}$ and the platform velocity unit vector $\hat{v}$) and the normal to the local terrain slope $\hat{n}$:

$$cos\, \psi \; = \hat{n} \cdot \hat{g} = \hat{n} \cdot (\hat{v} \times \hat{r}) \tag{5}$$

Figure 2-3 shows the geometry of a ground surface patch projected into a SAR image describing the relationship between the incidence angle θ, the local-incidence angle θ_i, and the projection angle ψ and the reference areas A_β, A_σ, and A_γ.

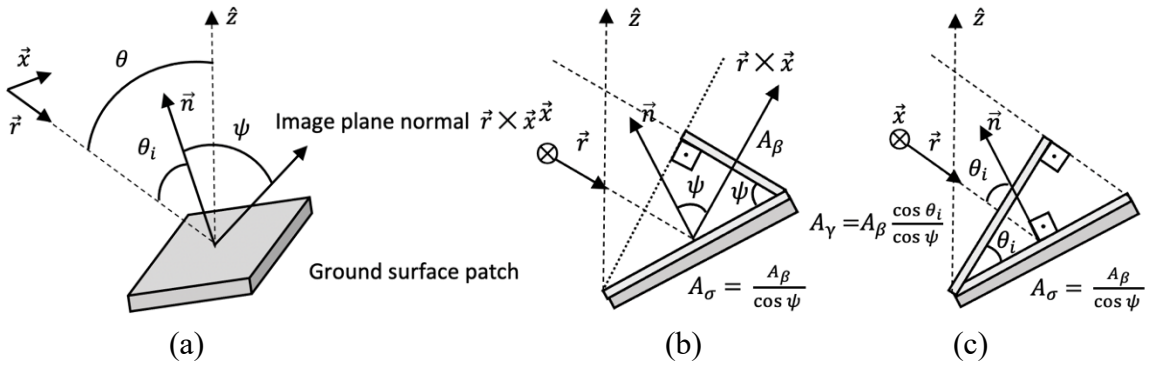

Figure 2-3. Diagrams illustrating the SAR imaging geometry of a ground surface patch (a) in the 3-D space, and in simplified 2-D planes describing the relationship between the (b) image reference surface A_β, and the ground surface A_σ and (c) the relationship between A_β, A_σ, and cross-section reference surface A_γ . $\vec{x}$ is the along-track vector, $\vec{r}$ is the look vector, $\vec{n}$ is the ground surface normal, θ is the ellipsoidal incidence angle, θ_i is the local-incidence angle, and ψ is the projection angle.

Since radar observations are given in the radar geometry, the transformations using the projection angle ψ and the local-incidence angle θ_i should also be resolved in the radar geometry. However, areas with *layover* and *foreshortening* may include backscatter from targets at different positions on the ground, representing a ``many-to-one" mapping. The existence of multiple geometries affecting a single radar sample hinders the estimation of a single projection angle ψ and the local-incidence angle θ_i that accurately represent the local geometry.

The RTC approach proposed by [D. Small, 2011] solves this problem by first computing the expected gamma-naught area A_γ in the geographic domain and further integrating the associated area over the radar grid so that the area contributions from different geographic positions are accounted for, even if they fall within the same radar grid bin. Each gamma-naught area element is obtained by measuring the ground surface area A_σ from reference DEM and scaling it to the gamma-naught area A_γ by projecting the facet onto the cross-section plane using the local-incidence angle. The resulting gamma-naught area is projected from the geographic domain onto the radar geometry, and accumulated over each pixel of the radar grid. Afterwards, the sum is divided by the beta-naught area A_β, and the resulting ratio, referred to as the *area normalization factor* (ANF), can then be used to scale the radar brightness β^0 to the backscatter coefficient γ^0 [Small, 2011, Shiroma et al. 2022].

The projection of the gamma-naught area from the geographical grid, or geogrid, onto the radar grid proposed by [Small, 2011] uses a bilinear distribution. This approach often requires high DEM upsampling to avoid aliasing effects and unwanted artifacts, especially in areas with steep topography. Unfortunately, the DEM upsampling usually comes with a polynomial cost (linear in each direction), significantly increasing the processing time. A more efficient approach uses the slant-range projection with the area projection algorithm [Shiroma et al, 2022]. This projection is

able to adapt to different postings between the geogrid and the radar grid, filling all spaces covered by the projected area elements without leaving gaps, reducing or, in some cases, eliminating the need for DEM upsampling.

2.3 The Area Projection Algorithm

The projection between radar and geographic coordinates, an operation shared by the radiometric terrain correction and geocoding steps, is traditionally performed by interpolation, which assumes the representation of data as point elements. However, radar samples often contain information gathered not only from a point but from the integrated area or volume delimited by the resolution cell associated with the samples. The area projection algorithm consists of handling pieces of data as area elements, rather than point elements [Shiroma et al, 2022]. Each area element in one coordinate system is associated with a number of area elements in the other coordinate system based on the elements' spatial extents. The values associated with the area elements are averaged and distributed from the source to the target grid. The number of averaged samples varies with the topography and data acquisition geometry. When applied to geocoding, the method represents an adaptive multi-looking that differs from the constant-window multi-looking that is traditionally applied to SAR data to reduce noise and speckle. Analogously, the slant-range projection of geocoded data is improved by projecting geographic grid pixels onto the radar grid according to their corresponding extents without leaving gaps. The slant-range projection with the area projection algorithm is used to significantly reduce the computation time of the radiometric terrain correction over previously published RTC algorithms [Shiroma et al, 2022].

2.3.1 Description of the Area Projection Algorithm

The first step of the area projection algorithm consists of dividing the geogrid into area elements to be mapped onto the radar geometry. For geocoding, the area elements are defined as the geographical grid pixels (i.e., squares or rectangles). The RTC-AP algorithm, implemented in ISCE3, utilizes triangles to represent these elements (see Section 2.3.4).

After defining the area elements, the algorithm starts by visiting each vertex of the area element *x* perimeter in the clockwise order. The position of the vertex over the radar grid is located through appropriate coordinate transformation to the radar geometry also known as *geo2rdr*. The projected polygon is then rasterized onto the radar grid through a polygon *rasterization algorithm*.

If the area element has more than three vertices, the projected polygon is tested for *self-intersection*. If the polygon is self-intersecting (e.g., antiparallelogram), the corresponding AE is subdivided into smaller sub-AEs (two triangles) and the process is repeated for each sub-AE [Shiroma et al, 2022].

The projected polygon is then rasterized onto the radar grid through a polygon *rasterization algorithm* (described in Section 2.3.2). The rasterized polygon will contain, for each *r*-th radar-grid pixel, weights $w_{r,x}$ whose absolute values range from $|w_{r,x}| = 0$, if it lies completely outside

the projected area element, and $|w_{r,x}| = 1$, if the pixel is fully contained inside the area element, and intermediate absolute values between 0 and 1 calculated based on the ratio of intersection between the radar-grid pixel and the projected area element (output of the rasterization algorithm).

2.3.2 Rasterization Algorithm

The suggested implementation of a rasterization algorithm is based on the integration of edges of a closed polygon. The polygon edges are represented as linear functions that can be integrated by definite integrals where the lower and upper limits are delimited by the polygon vertices. The algorithm is illustrated in Figure 2-4.

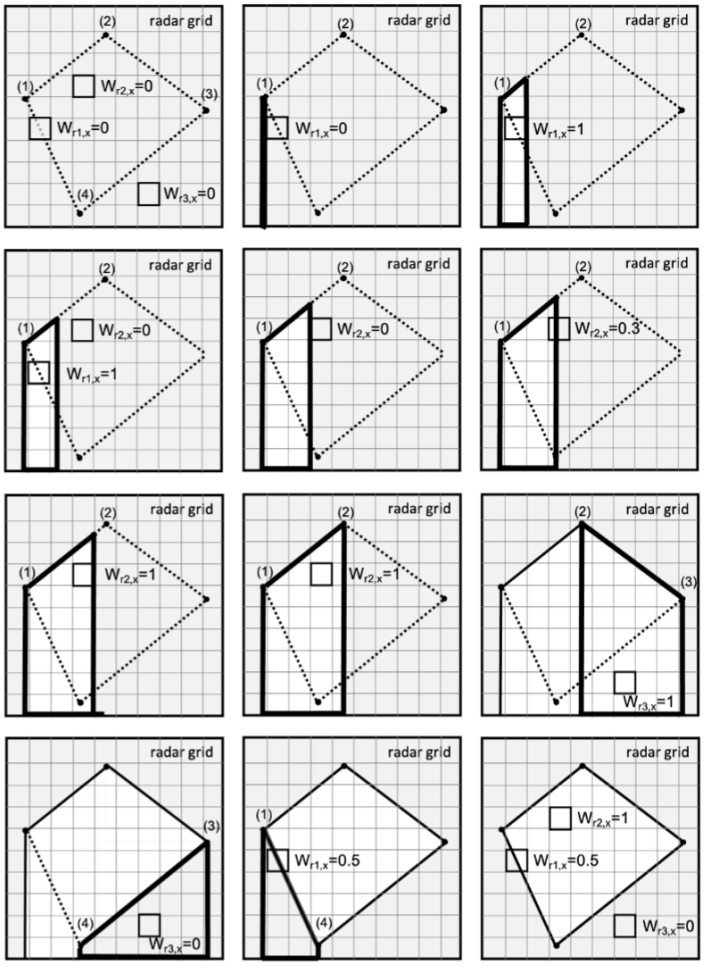

Figure 2-4. Rasterization algorithm implemented in ISCE3 based on the integration of a closed polygon. Each edge of the projected polygon is traversed in the clockwise order. To each pixel *r*, intersected by or below the edge, a value representing the fraction of intersection, varying from *0* to *1*, is added if the integration occurs from left to right, or subtracted otherwise. In the figure, this process is shown step-by-step between the edges associated with the vertices (1) and (2). The same process is repeated for the following edges. The integration stops when all edges are visited.

Since the edges are visited in the clockwise order, the integrated value will be nonnegative and the resulting weight $w_{r,x}$, associated with the area element *x* and radar-grid element *r*, will also be nonnegative ranging from *0* to *1*.

The suggested rasterization algorithm starts by successively traversing each edge of the area element in a predefined order. If the polygon is traversed in the clockwise direction, all weights and integrated values will be nonnegative. On the other hand, if the polygon is traversed in the anti-clockwise direction, all rasterized values and integrated area will be nonpositive. Therefore, the suggested rasterization algorithm also allows for testing the visiting order of the polygon edges. To each pixel *r*, intersected by or below the edge, a value representing the fraction of intersection, varying from *0* to *1*, is added if the integration occurs from left to right or subtracted, otherwise. The integration stops when all edges are visited.

Notice that one loop sequence iterates over the pixels intersected by the edge. For each intersection, another loop visits the pixels below the intersected pixel, adding the fraction of intersection as illustrated in Figure 2-4. Notice also that the same pixel may be visited multiple times while integrating a single edge or different edges. For instance, in Figure 2-4, the point $w_{r2,x}$, initially set to *0*, is updated to *0.3*, and successively to *1* during the integration of the first edge. The point $w_{r3,x}$ is set to *1* during the integration of the second edge and reset to *0* during the integration of the third edge.

2.3.3 Geocoding with Adaptive Multilooking (GEO-AP)

The association between radar grid pixels and geogrid area elements along with the corresponding weight map are used to project data from geo-coordinates to radar-grid coordinates and vice-versa.

If the projection occurs from the radar grid to the geo-coordinates, the geocoded value g_x is obtained from the weighted average of the set *R* of radar grid pixels *r* with value A_r that intersect completely or partially the area element *x*,

$$g_x = \frac{\sum_{r=1}^{R} |w_{r,x}| A_r}{\sum_{r=1}^{R} |w_{r,x}|} \tag{6}$$

The denominator of the equation above represents the number of looks n_x intersected by the area element *x*:

$$n_x = \sum_{r=1}^{R} |w_{r,x}| \tag{7}$$

Notice that n_x is often not an integer value and it varies with the shape of the area element *x* projected over the radar grid. Null radar samples or undefined elements should have their associated weights set to zero $w_{r,x} = 0$.

The weighted averaging performed by the proposed geocoding algorithm is equivalent to an adaptive multilooking operation that accounts for the topography and acquisition geometry. Notice also that this process does not require interpolation, resulting in a projection that is free

from interpolation errors such as overfitting, that commonly occur in high-contrast areas, such as urban areas for radar backscatter.

2.3.4 Area-Based Radiometric Terrain Correction (RTC-AP)

The area projection algorithm also allows for the projection in the inverse direction, i.e., from the data G_x, in geo-coordinates to the projected data A_r, in radar-grid coordinates. This operation, traditionally called *slant-range projection*, *inverse geocoding*, or *back geocoding*, is commonly employed for co-registering SAR images for interferometric purposes. The projected radar-grid value A_r is obtained by averaging or accumulating the projected values of G_x, associated with radar grid pixel r.

Since the slant-range projection with the AP algorithm is able to adapt to different postings between the geogrid and the radar grid while filling all intermediate spaces covered by the projected area elements without leaving gaps, it can be used to replace the slant-range projection performed by the bilinear distribution (RTC-BI). The area projection algorithm is then used to project and accumulate the gamma-naught area from the geo-coordinates onto the radar grid as [Shiroma et al. 2022]:

$$A_r \leftarrow A_r + \frac{|w_{r,x}| G_x}{\sum_{r'=1}^{R} |w_{r',x}|} \tag{8}$$

This new approach reduces or eliminates the need for DEM upsampling, which represents an important improvement of the RTC-AP algorithm over the traditional method, especially when the radar grid posting is much finer than the DEM posting (see Fig. 2-5). This improvement enables the radiometric terrain correction to be performed at the full SLC-resolution, which results in radar backscatter with higher accuracy and finer details.

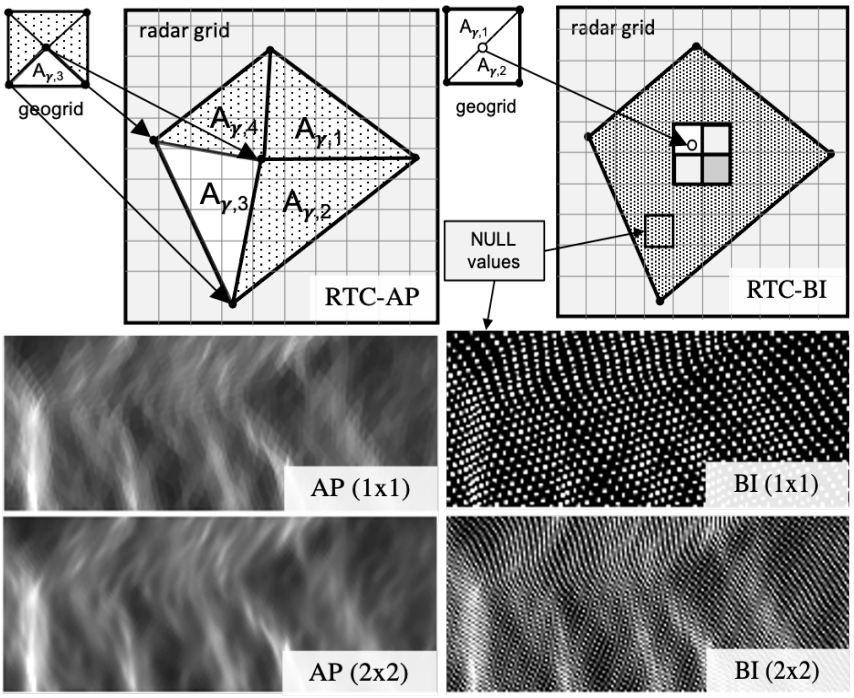

Figure 2-5. Diagrams illustrating the RTC with the (Top Left) bilinear distribution (RTC-BI) and (Top Right) AP (RTC-AP) algorithm, followed by images of the RTC ANF from NISAR-simulated single-look imagery (20-MHz mode) generated with the (Bottom Left) RTC-BI and (Bottom Right) RTC-AP algorithm. The level of DEM upsampling along easting and northing directions is indicated inside the parenthesis. The RTC-BI algorithm may leave gaps or suffer from aliasing effects, requiring higher DEM upsampling compared to the RTC-AP algorithm.

The first step of the algorithm is to determine the input geographical grid. In our implementation, we define the RTC geographical grid based on the output product grid, with pixel spacing set as a fraction of the output grid pixel spacing. We refer to this fraction as the RTC geogrid upsampling. For the OPERA RTC-S1 product, the RTC geogrid upsampling is set to *2* in both directions, i.e., (2x2). Since the OPERA RTC-S1 product has a pixel spacing of 30-m, the RTC geographical grid has pixel spacing of 15-m.

After the geographical grid is defined, each element of that grid is then subdivided into four triangular facets using the vertices and the center of the grid element (as shown in Fig. 2-5). Each of the four facets are visited, repeating the following steps:

1.1. Compute the cosine of the local-incidence angle $cos\ \theta_i$. If it is negative, the facet does not face the sensor and the execution skips to the next facet.

1.2. Measure the facet ground surface area A_σ^F , which can be obtained from the DEM using the cross-product area:

$$A_\sigma^F = \frac{\| \overrightarrow{e_1} \times \overrightarrow{e_2} \|}{2} \tag{9}$$

where $\overrightarrow{e_1}$ and $\overrightarrow{e_2}$ are two of the three edges of the facet (triangle).

Another option is to use the Heron's formula to calculate the area of a triangle [Small, 2011]:

$$h = \frac{1}{2} P_a + P_b + P_c \tag{10}$$

$$A_\sigma^F = \sqrt{h\,(h - P_a)(h - P_b)(h - P_c)} \tag{11}$$

where h is the facet semi-perimeter and P_a, P_b and P_c are the lengths of the edges, measured from the distance (in the three-dimensional space) between the facet vertices. The heights of the vertices are obtained from the reference DEM.

1.3. Scale the facet ground surface area A_σ^F to the facet gamma-naught area A_γ^F by projecting the facet area onto the cross-section plane using the local-incidence angle:

$$A_\gamma^F = A_\sigma^F \cos\theta_i \tag{12}$$

1.4. Run the rasterization algorithm (described in Section 2.3.2) to determine the association weights $w_{r,x}$.

1.5. Project and accumulate the gamma-naught area A_γ^F over the radar grid using the association weights $w_{r,x}$:

$$A_\gamma \leftarrow A_\gamma + \frac{|w_{r,x}| \,.\, A_\gamma^F}{\sum_{r'=1}^{R} |w_{r',x}|} \tag{13}$$

After the steps above are completed, for each radar-grid element, the accumulated gamma-naught area A_γ is divided by the beta-naught area A_β (i.e., the radar grid pixel area). The resulting ratio, referred to as the radiometric terrain correction area normalization factor (RTC ANF), can then be used to scale the radar brightness β^0 to the backscatter coefficient A_γ.

The RTC-ANF does not change with polarization as it is derived from radar imaging geometry. It is therefore applied to each polarization channel p of the input S1 SLC s_p:

$$g_{x,p}^\gamma = \frac{\sum_{r=1}^{R} |w_{r,x}| \frac{A_\beta}{A_\gamma} \left|s_p\right|^2}{\sum_{r=1}^{R} |w_{r,x}|} \tag{14}$$

2.4 Algorithm Inputs

The three inputs to the RTC-S1 algorithm are listed in Table 2-1. These inputs consist of:

- Sentinel-1 SLC (SAFE file):

  The S1 SAFE file for an Interferometric Wide (IW) swath mode of a S1 product contains individually focused SLC images (i.e., bursts) acquired by the European Space Agency (ESA) S1 sensors. The IW mode is the main acquisition mode over land and it acquires data with a 250 km swath at 5 m x 20 m spatial resolution (range x azimuth, single look). The IW mode captures 3 sub-swaths. All the bursts in all the three sub-swaths of an IW SLC product are resampled by ESA to a common pixel space grid in slant range and azimuth. The resampling to a common grid eliminates the need for further interpolation in later processing stages.

  In addition, the input SAFE file contains S1 metadata, usually distributed in annotation XML files. Particularly, these files include:

  - *Annotation files*: for all the three sub-swaths. These files contain basic processing information for each burst including the burst of interest.
  - *Calibration annotation files*: for all the three sub-swaths. These files contain information to perform radiometric calibration of the S1 bursts.
  - *Noise annotation file*: for all the three sub-swaths. These files contain information to perform the thermal denoising of the S1 bursts.
  - *Radio Frequency Interference (RFI) annotation files*: for all the three sub-swaths. These files contain information on the RFI detection and mitigation strategy adopted by the Sentinel-1 Instrument Processing Facility (IPF).

- Sentinel-1 Orbit Ephemerides:

  The S1 orbit ephemerides files contain information on the S1 satellites' position and velocity recorded by a Global Navigation Satellite System (GNSS) during the sensor acquisition. S1 product orbit information generated by an on-board navigation solution are stored within the S1 Level-1 products. The orbit positions are later refined by the Copernicus Precise Orbit Determination (POD) Service.

  S1 orbit ephemerides files are available in the form of:

  - Precise Orbit Ephemerides (POE): delivered within 20 days after the S1 data acquisition and exhibiting less than 5 cm accuracy.
  - Restituted Orbit Ephemerides (ROE): delivered within 3 hours after the S1 acquisition and exhibiting less than 10 cm accuracy.

  The orbit ephemeris files can be downloaded through ESA Scihub or alternatively through Alaska Satellite Facility (ASF) website.

- Digital Elevation Model (DEM):

  The SAS uses the project-specified DEM for processing based on the Copernicus DEM 30-m (GLO-30 DEM) and 90-m (GLO-30 DEM), provided by the European Space Agency. The DEM is the same as prepared for the NASA-ISRO Synthetic Aperture Radar mission, referred to as the NISAR-DEM.

Table 2-1. Inputs to the RTC-S1 algorithm.

Input Data	Producer
Sentinel-1 SLC	ESA
Sentinel-1 Orbit Ephemerides	ESA
Copernicus GLO-30 and GLO-90 DEM	ESA

2.5 Algorithm Outputs

Table 2-2 lists all output layers (bands) of the RTC-S1 algorithm. The layers VV and VH contain the RTC-S1 backscatter, i.e., the SAR backscatter normalized to gamma-naught, of the VV and VH polarization channels, respectively.

As explained in Sec. 1.2, some radar geometry layers vary slightly over time for each position on the ground and therefore are considered static for the project. These static layers are provided as the OPERA RTC-S1 static layers (RTC-S1-STATIC) product, separately from the RTC-S1 product. RTC-S1-STATIC products are produced only once or a limited number of times, to account for changes in the S1 orbit, in the DEM, or in the static-layers generation algorithm. The RTC-S1-STATIC product includes the following layers number of looks (“number_of_looks”), RTC ANF gamma0 to beta0 (“rtc_anf_gamma0_to_beta0”), RTC ANF gamma0 to sigma0 (“rtc_anf_gamma0_to_sigma0”), incidence angle (“incidence_angle”), and local incidence angle (“local_incidence_angle”)

The mask layer provide a layover/shadow mask classification and it is included in both products RTC-S1 and RTC-S1-STATIC.

Table 2-2. Output layers of the OPERA RTC-S1 product.

Product	Band Name	Band Description
RTC-S1	VV	Radiometric terrain-corrected VV backscatter normalized to gamma-naught
RTC-S1	VH	Radiometric terrain-corrected VH backscatter normalized to gamma-naught
RTC-S1	mask	Layover/shadow mask
RTC-S1-STATIC	number_of_looks	Number of averaged radar-grid pixels for each RTC-S1 backscatter estimation
RTC-S1-STATIC	rtc_anf_gamma0_to_beta0	Area normalization factor from beta0 to gamma0 using DEM
RTC-S1-STATIC	rtc_anf_gamma0_to_sigma0	Area normalization factor from beta0 to gamma0 using DEM
RTC-S1-STATIC	incidence_angle	Incidence angle is defined as angle between LOS vector and geodetic normal at the target
RTC-S1-STATIC	local_incidence_angle	Local-incidence angle is defined as angle between LOS vector and terrain normal at the target
RTC-S1-STATIC	mask	Layover/shadow mask

3 ALGORITHM ASSUMPTIONS

It is assumed that the reference DEM based on the Copernicus DEM 30m and 90m, used in the RTC-S1 radiometric terrain correction and geocoding, provides a good representation of the local topography.

Also, RTC-S1 products are not corrected for ionospheric shifts. It is assumed that ionospheric geolocation errors are relatively small for C-band backscatter sampled at 30m x 30m.

4 ALGORITHM IMPLEMENTATION

The OPERA RTC-S1 product workflow is developed by the OPERA Algorithm Development Team (ADT). It is implemented in Python and it is open-source accessed through the following GitHub repository:

https://github.com/opera-adt/RTC

The software has two main dependencies. The algorithm's core modules are implemented within the ISCE3 in C++ with Python bindings that expose the GeocodeCov and GetRadarGrid modules that are required by the OPERA RTC-S1 workflow. ISCE3 is open-source and it is available at:

https://github.com/isce-framework/isce3

The second main dependency is the OPERA S1-Reader. The S1-Reader is the software that parses the S1 metadata and instantiate the objects that are required by ISCE3. The OPERA S1-Reader is also open-source and it is available at:

https://github.com/opera-adt/s1-reader

5 ALGORITHM USAGE CONSTRAINTS

The algorithm does not account for:

- Errors due to Radio Frequency Interference (RFI). Some RFI metadata provided with Sentinel-1 annotation files are copied to RTC-S1 products. However, RFI errors are not corrected or mitigated by the RTC-S1 algorithm.
- Processing of Sentinel-1 Ground Range Detected (GRD) products. The algorithm is only applicable to Single-look Complex (SLC) data.
- Geolocation errors caused by ionospheric effects.
- Errors in the existing DEMs that can cause geolocation errors and artifacts added into the RTC-S1 imagery due errors in the radiometric terrain correction;

6 PERFORMANCE ASSESSMENT

The OPERA RTC-S1 algorithm and product are evaluated through a 2-step process. The algorithm verification is performed in the development phase and it encompasses a broader set of tests compared to the product validation. It ensures that the algorithm is able to, not only meet the project requirements, but also provide products with highest quality and accuracy for given project's constraints (e.g., storage costs and processing capabilities). The product validation, on the other hand, verifies if the product meets the project requirements. Algorithm verification activities include [Shiroma et al., 2023]:

- Comparison of the RTC area normalization factor (ANF) applied to the RTC-S1 images using the RTC-AP algorithm with the RTC ANF obtained from other algorithms [Shiroma et al. 2022].
- Comparison of ISCE3 processed imagery with those obtained from other software.
- Assessment of the dependence of the RTC-S1 backscatter with respect to the topography for different target types and polarizations - An RTC study has been carried out using 46 S1 datasets [Rosario et al., 2023].
- Evaluation of the RTC/geocoding algorithm over ascending and descending tracks and over neighboring swaths [Shiroma et al. 2022].
- Evaluation of the geolocation using corner reflectors.
- Verification of the product format with respect to the product specification.
- Assessment of the workflow run time and memory usage.
- Verification of the metadata with respect to the RTC-S1 product specification [Shiroma et al., 2023].

Product validation activities include:

- End-to-end global run test for a Sentinel-1A orbit cycle (Figure 1-2).
- Assessment of absolute and relative geolocation errors.
- Evaluation of the linear regression of the RTC-S1 backscatter against the local incidence angle in forested areas.
- Comparison of the radar backscatter over foreslope and backslope areas.

7 DATA ACCESS

Data Access Input Data:

- Sentinel-1 IW SLC files.
- Sentinel-1 Orbit files.
- Copernicus DEM GLO-30 and GLO-90.

Data Access Output Data:

- RTC-S1 and RTC-S1-STATIC products are available through the NASA ASF-DAAC.

Data Access Related URLs:

- Copernicus DEM GLO-30 and GLO-90: https://doi.org/10.5270/ESA-c5d3d65.

8 CONTACTS

Gustavo H. X. Shiroma
OPERA Algorithm Development Team (ADT)
Jet Propulsion Laboratory, California Institute of Technology
Pasadena, CA, USA
gustavo.h.shiroma@jpl.nasa.gov

9 REFERENCES

Agram, P. S., Warren, M. S., Arko, S. A., and Calef, M. T., "Radiometric terrain flattening of geocoded stacks of SAR imagery," Remote Sensing, vol. 15, no. 7, 2023.

Shiroma, G. H. X., Lavalle, M., and Buckley, S., "An Area-Based Projection Algorithm for SAR Radiometric Terrain Correction and Geocoding," in IEEE Transactions on Geoscience and Remote Sensing, vol. 60, pp. 1-23, 2022, Art no. 5222723, doi: 10.1109/TGRS.2022.3147472.

Miranda, N., and Meadows, P. J., "Radiometric Calibration of S-1 Level-1 Products Generated by the S-1 IPF,", 2015, ESA document. Accessed: 2024-06-24. [Online]. Available: https://sentinel.esa.int/documents/247904/685163/s1-radiometric-calibration-v1.0.pdf.

Piantanida, R., Miranda, N., Franceschi, N., and Meadows, P., "Thermal Denoising of Products Generated by the S-1 IPF", 2017.

Gisinger, C., Schubert, A., Breit, H., Garthwaite, M., Balss, U., Willberg, M., Small, D., Eineder, and M., Miranda, N., "In- Depth Verification of Sentinel-1 and TerraSAR-X Geolocation Accuracy Using the Australian Corner Reflector Array," IEEE Transactions on Geoscience and Remote Sensing, vol. 59, no. 2, pp. 1154–1181, 2021.

Breit, H., Fritz, T., Balss, U., Lachaise, M., Niedermeier A., and Vonavka, M., "TerraSAR-X SAR Processing and Products," IEEE Transactions on Geoscience and

Small, D. "Flattening gamma: Radiometric terrain correction for SAR imagery," IEEE Trans. Geosci. Remote Sens., vol. 49, no. 8, pp. 3081–3093, Aug. 2011.

Ulaby, F. T., Moore, R. K., and Fung, A. K., "Microwave Remote Sensing: Active and Passive Vol III: From Theory to Applications", Artech House, 1986

Ulander, L. M. H., "Radiometric slope correction of synthetic-aperture radar images," IEEE Trans. Geosci. Remote Sens., vol. 34, no. 5, pp. 1115–1122, Sep. 1996.

Rosario, J., Shiroma, G. H. X., Fattahi, H., Meyer, F., and Jeong, S., "Assessment of Terrain Dependence of Radiometric Terrain Corrected C-Band Sentinel-1 SAR Backscatter over Different Target Types," IGARSS 2023 - 2023 IEEE International Geoscience and Remote Sensing Symposium, Pasadena, CA, USA, 2023, pp. 4286-4289, doi: 10.1109/IGARSS52108.2023.10281744.

Shiroma, G. H. X., Fattahi, H., Meyer, F., Jeong, S., Cinquini L., Collins, S., Chapman, B., Chan, S. K., Handwerger, A. L., and Bekaert, D., "The Opera Radiometric Terrain Corrected Sar Backscatter from Sentinel-1 (RTC-S1) Product," IGARSS 2023 - 2023 IEEE International Geoscience and Remote Sensing Symposium, Pasadena, CA, USA, 2023, pp. 880-883, doi: 10.1109/IGARSS52108.2023.10282385.

ACKNOWLEDGEMENTS

This research was conducted at the Jet Propulsion Laboratory, California Institute of Technology, under contract with the National Aeronautics and Space Administration. The original Copernicus Sentinel data used in this document have been provided by the European Space Agency (ESA).